# A Preliminary Evaluation of Static Tests to Detect Slip Using Tyre Strain Sensing System in Robotic Platforms

Ali Farooq Lutfi Lutfi, Tobias Low, and Andrew Maxwell

***Abstract*— Wheel slip estimation is a determinant factor in improving performance of wheeled vehicles. Conventional wheel slip estimation methods relied upon sensors which are far from the tyre-ground interface; hence, they required the use of approximated models and complex transformations. A modern method which directly measures tyre-ground contact quantities utilising in-tyre sensors helps develop accurate and direct wheel slip estimation techniques. In this paper, an optimum sensing system for small, non-pressurised robotic tyres is presented. Data processing algorithms are proposed to show possible techniques for deploying the readings of this system to estimate tyre forces and slip variables. These algorithms analyse the sensing system's measurements in both longitudinal and lateral directions with respect to the tyre direction of motion. Performance of the system is evaluated with static tests using a custom-built, bench-top rig. In these tests, different angular positions, vertical forces, and horizontal forces were tested. Results of these tests demonstrated that the system is capable of detecting tyre slip with a suffcient degree of consistency and robustness.**

## I. INTRODUCTION

Wheel slip represents an important element in a number of applications for both robots and cars. Regarding wheeled mobile robots, odometric solutions produce false position estimations during wheel slip incidents [1]. In addition, taking wheel slip into consideration is a crucial element in developing efficient path planning algorithms [2]. Moreover, wheel slip estimation is a key component in enhancing various control systems, such as traction control and stability control [3]. Also, wheel slip affects the navigation of the mobile robot and hinders its performance in target chasing and obstacle avoidance. Furthermore, as it does not contribute to the desired robot's motion in the planned path, wheel slip is regarded as a form of energy loss. Thus, wheel slip estimation results in a reduction of the robot's energy consumption. In the automotive literature, the relationship between the wheel slip and the tyre-road friction has been deployed to obtain critical information. For example, the friction coefficient-slip curve was utilised to estimate the maximum tyre-road friction coefficient and to detect slippery regions in the road. Also, wheel slip is an important parameter in several active safety systems [4].

Conventional wheel slip estimation methods based on different sensors such as accelerometers, gyros, IMU, and cameras have been proposed [5], [1], [3]. These sensors were mounted on different positions on the body of the vehicle. Hence, to interpret the indirect measurements collected by these sensors about the tyre-ground dynamic events, a number of projections from one coordinate system to another as well as imprecise mathematical models were required [6]. However, because of developing sensor technologies, it is possible now to embed various types of sensors in the tyre to directly measure different tyre-ground quantities [7].

It is argued that a significant improvement to wheel slip estimation approaches could be achieved by developing in-tyre sensory systems. The reason is that tyres produce nearly all forces and moments experienced by the vehicle [8]. To estimate these quantities, a tyre being converted into a sensing unit outperforms other solutions in terms of direct detection of variations, high robustness, and close proximity to the interface area. Moreover, Erdogan et al. [9] suggested that tyre sensors can deliver reliable readings even under normal, steady state driving which is generally not the case with standard vehicle sensors. Therefore, utilising such systems, measurements, which are direct, real-time, and as close to the tyre contact patch as possible could be collected and deployed for accurate wheel slip detection.

This paper presents an in-tyre sensing system which can accurately measure tyre-ground interactions for robotic platforms. It also proposes data processing algorithms to estimate tyre forces and slip variables in both longitudinal and lateral directios with respect to the tyre direction of motion. Static tests on a custom-built, bench-top rig are conducted to assess the performance of the implemented sensing system in detecting wheel slip.

## II. TYRE STRAIN SENSING SYSTEM FOR A ROBOTIC PLATFORM

The main components for building a tyre strain sensing system for a robotic platform are identifying an appropriate sensing system, chosing suitable sensors, selecting a wheel/tyre to facilitate the installation process, suggesting an optimum sensor system design, and building a data acquisition system.

Tyre sensing systems in both the automotive and robotic fields were examined to suggest an appropriate system for small, non-pressurised robotic tyres. It was concluded that various sensor types, technologies, and configurations were presented to develop tyre deformation sensing systems [10], [11], [12], [13], [14]. Taking into account the cost, complexity, availability, compatibility with tyre material, and size, contacting strain sensing utilising a flexible sensor

This work was supported by University of Southern Queensland, Australia

A. Lutfi, T. Low, and A. Maxwell are with Faculty of Health, Engineering and Sciences, University of Southern Queensland, Australia {AliFarooqLutfi.Lutfi, Tobias.Low, Andrew.Maxwell}@usq.edu.au

A. Lutfi is with Control and Systems Engineering Department, University of Technology, Baghdad, Iraq

is suggested for this research. Two possible options were identified for mounting sensors inside tyres either gluing on the inner tyre surface or embedding in the tyre tread. In this study, the contacting sensors will be glued on the tyre inner surface as the other option is more difficult to be positioned properly and may not provide useful data due to the relative motion between the sensor and the tyre throughout the contact patch [15].

The strain gauges utilised for this research were from Micro-Measurements division (Measurements group, INC.). The gauges type is CEA-06-240UZ-120 Student Gauges. The resistance of the gauge in ohms is $120.0 \pm 0.3\%$ and the gauge factor is $2.070 \pm 0.5\%$ at $24°$C. These low-cost, general-purpose, experimentally widely used gauges are extremely thin, 0.056 mm, and flexible. For static strain readings, they operate in a temperature range from $-75°$ to $+175°$C. For single cycle use, these high-elongation gauges can measure up to $5\%$ elongation. To reduce thermal effects to least possible levels, self-temperature compensation (STC) characteristics were added to the gauges during the production process. All these features make these sensors an ideal solution for developing a sensing system inside a robotic tyre. In this context, it should be affirmed that designing a special sensor is out of the scope of this work. However, designing a new tyre sensing system, in terms of sensors type, number, and configuration, is indispensable to reach the specific research objectives.

The tyre utilised for this study can be used for a robotic platform called CoroBot Explorer. Traditionally, the tyres that are used with this platform are fused to the wheel with a very strong adhesive. Since the application of in-tyre sensors requires the ability to easily get the tyres off the wheels, the standard tyres were not helpful and the best solution was to use the so called bead-lock rims. In these wheels, the tyre is fixed to the wheel with a bead-lock ring which is secured using screws to fix the tyre edge to the rim. The wheel is about 89 mm in inner diameter, 113 mm in outer diameter, and 83 mm in width. The tyres are non-pressurised, i.e., they use foam inserts instead of air. This type of tyres is commonly used for robotic platforms. The tyre is about 95 mm in inner diameter, 139 mm in outer diameter, 87 mm in width, and 10 mm in sidewall height.

To suggest an optimum design of the sensory system for the particular tyre used herein, compression tests (footprint tests) were conducted using a compression machine. These tests helped in studying the contact patch in terms of its shape (contour) as well as the effect of changing the vertical force on varying its shape and size. From the results of these tests, it was decided to place the sensor system in an area which corresponds to the smallest possible footprint, resulted from a vertical load of 10 N. This engineering decision was driven by the fact that this is a reasonable loading for small to medium-sized robots and by the available space inside the tyre. With this placement, it is ensured that all the sensors are located inside the area of the contact patch under all possible loading conditions.

To decide the most appropriate sensor system design, some criteria were placed. Most importantly, it must be able to capture measurements reflecting the strain distribution in both longitudinal and lateral directions. The reason for that was to cover the possible cases of tyre braking, traction, and turning (cornering). Other factors which affected the decision were the tyre dimensions, the minimum number of required sensors, and the best points to position the sensors. Fig. 1 presents the sensor design which is proposed to meet the requiremets of this work. It consists of six strain gauges glued on the tyre inner surface. In details, it contains three pairs of strain gauges where, in each pair, one strain gauge is placed longitudinally while the other is placed laterally with respect to the tyre direction of rotation. One pair is mounted on the tyre centreline while the other two pairs are placed symmetrically about the centreline. The sensors' positions were determined based on the dimensions of the selected footprint which resulted from the compression tests.

Finally, a data acquisition system based on National Instruments hardware and LabVIEW software was built to collect the sensors' readings. It consists of NI cDAQ-9172, NI 9219, and LabVIEW 2014. The built-in quarter-bridge configuration of NI 9219 was used. Wires are used to access the data from inside the tyre during the tests.

## III. PROCESSING TYRE STRAIN DATA TO EXTRACT FORCE AND SLIP VARIABLES

Measurements of in-tyre strain in the longitudinal (circumferential) direction and in the lateral (axial) direction can be utilised to derive respective force and slip variables. In the longitudinal direction, the sensors' measurements are analysed to calculate the longitudinal force ($F_x$) and the longitudinal slip ($\kappa$), which are required to represent the force-slip relationship. As can be seen in Fig. 2, the key element in the proposed processing algorithm is to determine the angular positions of the contact patch edges. This is performed by differentiating the longitudinal strain profile measured by a longitudinal strain senor. As shown in Fig. 3, two peaks in this time derivative waveform represent the leading edge ($x_l$) and trailing edge ($x_t$) of the contact patch.

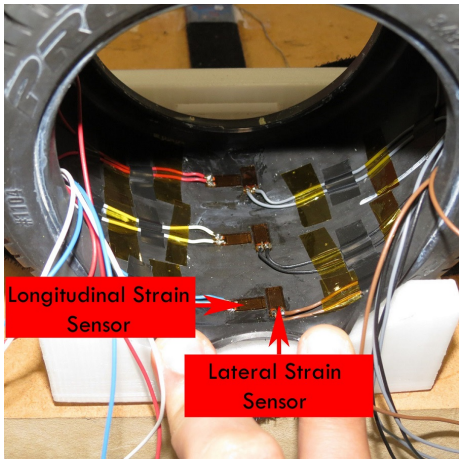


Fig. 1. The sensor system mounted to the tyre inner surface.

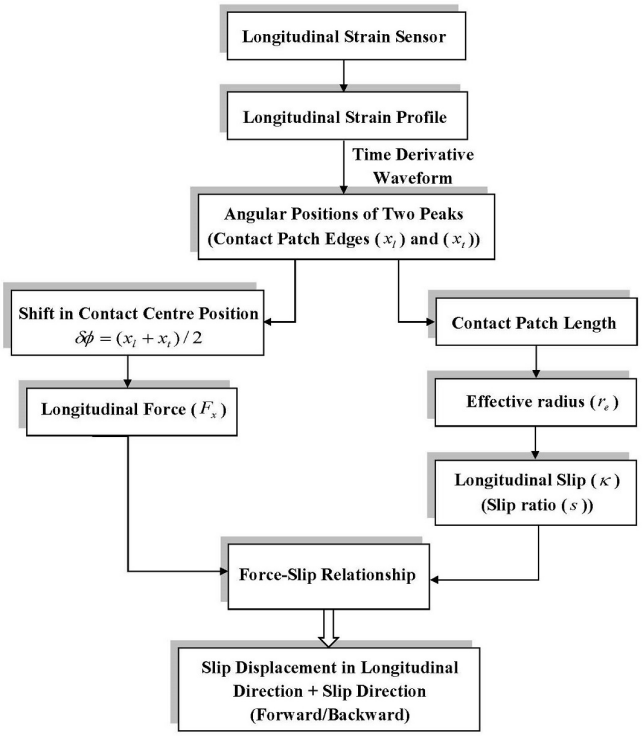


Fig. 2. Processing of sensors data in longitudinal direction.

After that, the longitudinal force ($F_x$) and the longitudinal slip ($\kappa$) (slip ratio ($s$)) are determined. Firstly, according to [16] and [6], the shift in the angular position of the contact patch centre ($\delta\phi = (x_l + x_t)/2$) is strongly related to the longitudinal force; therefore, ($F_x$) can be estimated. To calculate the longitudinal slip, the contact patch length, which is the distance between ($x_l$) and ($x_t$), is used to derive the effective radius ($r_e$). The contact patch length is linearly and inversely proportional to the effective radius [17]. Then, the value of the estimated effective radius is inserted into the following equation to calculate the longitudinal slip:

$$s = \frac{V - \omega r_e}{V} \tag{1}$$

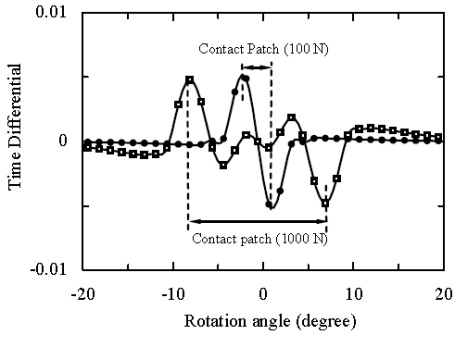


Fig. 3. Example for determining the contact patch edges for two values of wheel load [17].

Where ($V$) is the robot's linear velocity and ($\omega$) represents the wheel angular velocity.

It is also worthwhile to mention that there is a proportional relationship between the contact patch length and the vertical load; therefore, finding the patch length leads to estimating the applied vertical force.

Having obtained both ($F_x$) and ($s$), the force-slip relationship can now be constructed. Even though there exists a number of empirical models to describe this function, the most widely accepted expression is the Magic Formula [18]. The slippage displacement and direction will be estimated from this force-slip curve.

In the lateral direction, the lateral strain profile is acquired from the sensors' readings to define the force-slip relationship, as demonstrated in Fig. 4. Then, the slip angle ($\alpha$) is derived by applying a curve-fitting technique to the lateral profile. Also, the lateral force ($F_y$) is obtained from the deflection curve utilising a lateral deflection model [9]. Alternatively, since $F_y$ causes a variation in lateral strain distribution across the width of the contact patch, $F_y$ can be estimated from the difference in strain between the edges of the contact patch in the lateral direction [19].

As the slip angle and the lateral force have been estimated, the function relates the lateral force to the slip angle can now be represented using the Magic Formula. As previously stated, this force-slip relationship will be analysed to determine the slip displacement and direction in the lateral axis.

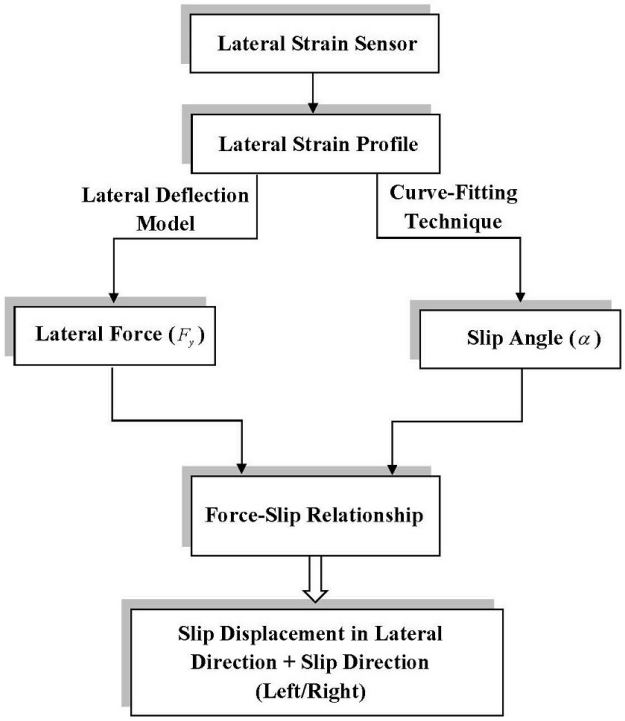


Fig. 4. Processing of sensors data in lateral direction.

## IV. TYRE TESTING BENCH-TOP RIG

A single-wheel, bench-top test rig was built to examine the performance of the in-tyre strain sensors using static tests. As seen in Fig. 5, different vertical forces, horizonal forces, and angular positions can be tested with this rig.

The rig consists of a board (50cm*50cm*1.7cm), 3D printed parts, Aluminium clamp, bolts, screws, and bearings. Four corner stands and one central stand hold the board on a bench. A vertical load block, which is a 3D printed bracket with a track attached to its base and a bolt which passes through a hole in its upper part, is used to apply vertical forces to the tyre. By turning the bolt, a slide is pushed towards the tyre in the radial direction. A horizontal load block, which has exactly the same design as the vertical load block, is used to apply horizontal forces on the tyre by directly pushing the slide in the horizontal direction with respect to the tyre contact patch. A slide holder, a 3D printed part which moves along the track of the vertical load block, is designed to enable the slide to move both vertically and horizontally with respect to the tyre contact patch. To build the sliding mechanism, a group of bearings, bolts, and threaded rods were placed inside the slide holder. The slide is a wooden board (250mm, 120mm, 17mm) which is placed on the bearings of the slide holder. It is used to apply vertical and horizontal forces to the tyre. A tyre holder, which is a cylinder with four screw holes to screw the part to the board and a central bolt hole, is used to hold the tyre. A big bolt passes through the centre of the wheel to the central hole in the tyre holder and to the board. A custom-designed Aluminium clamp is built to hold the tyre at different angular positions. As seen in Fig 5, this clamp was fixed at one end to the wheel, through four screws in the bead-lock rim, and at the other end to the board. To fix the tyre at different angles, the clamp was moved and screwed to the board at specified positions. Two compression load cells (FC2231-0000-0025-L) from TE Connectivity are used to measure the applied vertical and horizontal loads. The first load cell was placed on the slide holder to measure the applied vertical force while the second cell was placed at the edge of the slide to measure the horizontal forces. As the bolts, used to push the slide vertically and horizontally, make contact with the load cells, they read the corresponding vertical and horizontal forces.

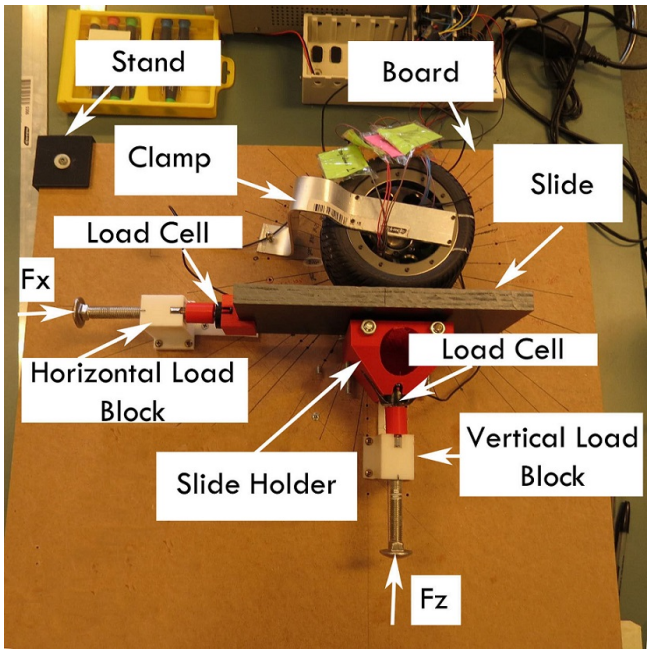


Fig. 5. Tyre bench-top rig used for static tests.

## V. STATIC TESTS TO DETECT SLIP

First, an unloaded test was conducted to record the bias readings of the sensors. The slide used in the bench-top rig was lifted so that no vertical or horizontal forces are exerted on the tyre. Knowing the bias values of the sensors is useful in analysing results of the next tests. As shown in Fig. 6, the readings were filtered using a Savitzky-Golay Filter where the polynomial order was three and the frame size was fifteen. The purpose of filtering was to slightly smooth the data without losing existing features.

As seen in Fig. 7, the value of the default strain measured by one sensor is slightly different from the readings of the other sensors. This is the result of different mounting positions for the six sensors with respect to the curvature of the tyre inner surface. Another reason is the different strains caused by gluing, soldering, and wiring of each sensor. For example, due to a limited available space, a strain relief loop was created in a way which is not exactly the same for all the sensors. Therefore, each sensor is originally stretched to a degree which is not the same for the other sensors.

A second set of tests was conducted to examine the sensors' response during slip incidents. These tests aimed at investigating imitated real-life situations of a running tyre. In these situations, the tyre rotates, experiences possible changes in wheel load due to variation in road surface, and encounters potential sudden forces in its circumferential

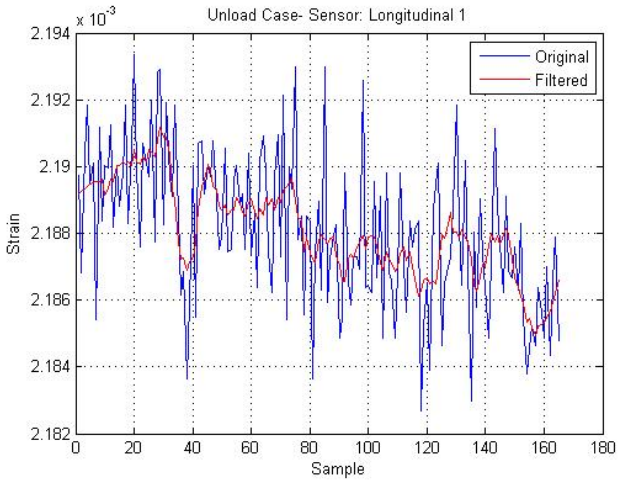


Fig. 6. Filtering the bias readings of the sensors (Example: Sensor-Longitudinal 1).

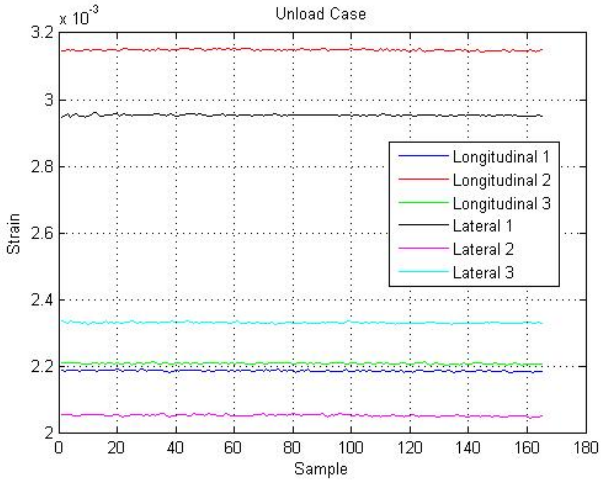


Fig. 7. Bias readings of the sensors.

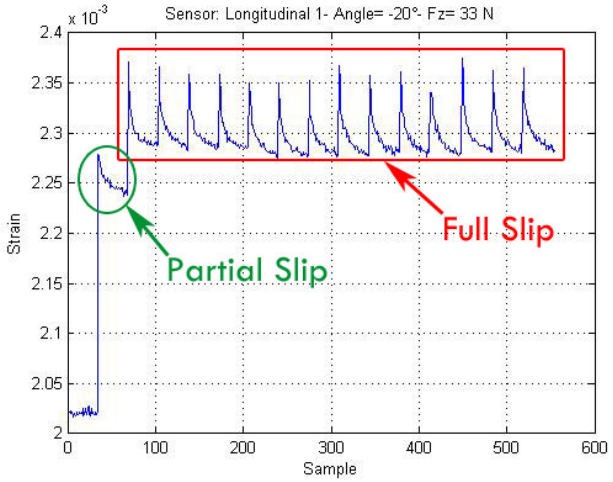


Fig. 8. Slip region detected in a longitudinal sensor's readings.

direction of motion as a result of braking or traction. Hence, performance of the sensors in response to changes in angular position, vertical force, and horizontal force was examined. In each of these tests, the tyre was fixed at a certain angle, a constant vertical force was applied, and the value of the horizontal force (Fx) was changed by increasing the number of bolt turns from 0 to 15 turns in steps of 1 turn. A fixed time was left before applying each turn. The direction of applying Fx was from left to right.

These tests were repeated for 13 angular positions, from 120° to -120° in steps of 20°, with three values of vertical force, Fz= 33 N, 44 N, or 60 N, in each angle. With respect to the centre of the contact patch, the positive angles are to the right-hand side while the negative angles are to the left-hand side. The most important angles are between 30° and −30°. This region is in the vicinity of the contact patch, ie, before entering the contact patch, in the contact patch, and after leaving the contact patch. It is expected that the strain variation will be more significant in this region compared to other angular positions where the sensors are far from the contact patch. It was not possible to examine angles which lie outside the previously mentioned range as the clamp, used to fix the tyre at these angles, would be blocked by other parts of the rig. Considering another limitation, choosing a smaller angular increment would have led to drilling more holes in the board to fix the tyre. Consequently, this would have resulted in a weak structure which is unable to bear the applied forces and subsequent motions of the rig's components.

## VI. EXPERIMENTAL RESULTS AND DISCUSSION

Fig. 8 and Fig. 9 show a longitudinal and a lateral sensor's readings, respectively, for one of the tests. A weighted moving average filter was applied to smooth the data without manipulating its real features so that the instantaneous variations caused by applying Fx remain easily traceable in the measurements. Thus, a Savitzky-Golay filter, where the polynomial order is four and the frame size is nineteen, was utilized. Inconsistencies in the results are caused by the amount of vibrations resulted from manual applications of the horizontal forces as well as from the sliding mechanism of the rig.

It is noticed in Fig. 8 and Fig. 9 that each application of a bolt turn in the longitudinal direction of tyre motion introduces a change (a spike) in the readings captured by the strain sensors. To explain, the tyre endures significant changes in strains as the longitudinal force is being applied then it enters a relatively constant-strain region. This sensor's reading is attributed to the way the used non-pressurised tyre responds to external loads. To clarify, the foam, planted inside the tyre, is compressed during the application of the force then it tries to regain its original position after the external load is no longer applied. However, the strain will not return to its starting value because the tyre is still compressed. In addition, the inherent hyperelastic behaviour in rubber greatly contributes to this result.

Another observation about the readings in Fig. 8 and Fig. 9 is that the change in the longitudinal strain is opposite to that of the lateral strain. In other words, the longitudinal

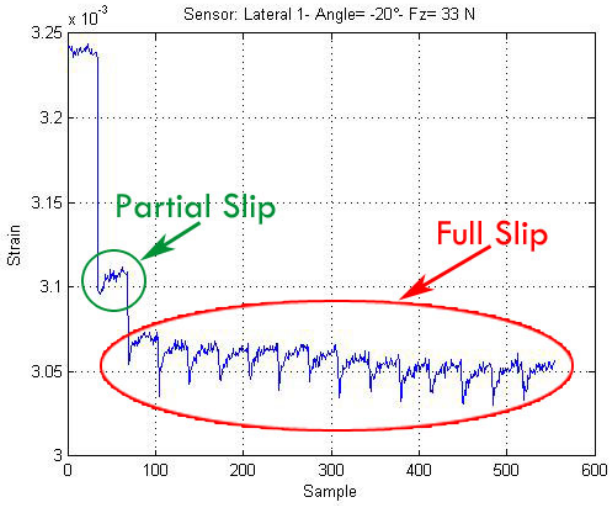


Fig. 9. Slip regions detected in a lateral sensor's readings.

sensor's readings provide an ascending shape whereas the lateral sensor's readings reflect a descending trend.

Fig. 10 and Fig. 11 show the relationship between the horizontal load and the strain at a specific vertical load and a specific angle. The first part in these figures demonstrates a linear relationship which indicates that the tyre is trying to adapt its structure according to the applied horizontal load. As a result, there is no slipping. This part is followed by a small region of nonlinearity where for one value of the horizontal load there are at least two values of strain. This area represents a region of partial slip. As the value of the horizontal load increases, the tyre is able to get out of this region, i.e., to recover from this partial slip situation. However, when the horizontal load exceeds a certain limit, the tyre completely slips. This full slip region is where the strain saturates. This fact plus the effect of the foam inside the tyre causes the strain readings to oscillate between a saturated limit, while applying the horizontal load, and a steady state limit, after removing the horizontal load in this region. In the sensors readings (Fig. 8 and Fig. 9), the full slip region is identified by a repeated pattern where the output starts to repeat itself when applying Fx because the tyre has already entered the slip stage. In other words, after entering this region, each time a horizontal load is applied, the strain reaches a saturated level then due to the non-pressurised property of the tyre, the strain returns to a steady state value when the horizontal load is lifted. Thus, the full slip situation can be detected using the raw sensors' readings or the relationship between the horizontal load and the strain value measured by the sensors.

The previous observations were confirmed by carefully examining successive screenshots from a video recorded for one of these tests. Fig. 12- Fig. 14 show examples of these screenshots. First, when applying small values of Fx, i.e., at the beginning of the test, the tyre tread blocks try to grip contact with the slide by moving in the same direction of applying Fx. In other words, in the beginning, there is no

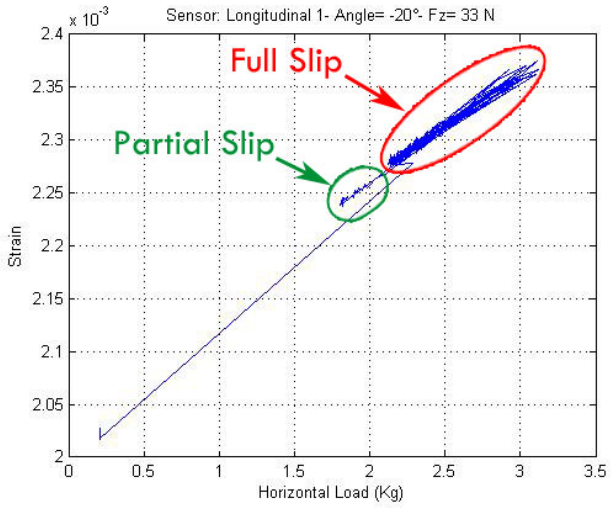


Fig. 10. Slip region detected in the horizontal load- strain relationship for a longitudinal sensor.

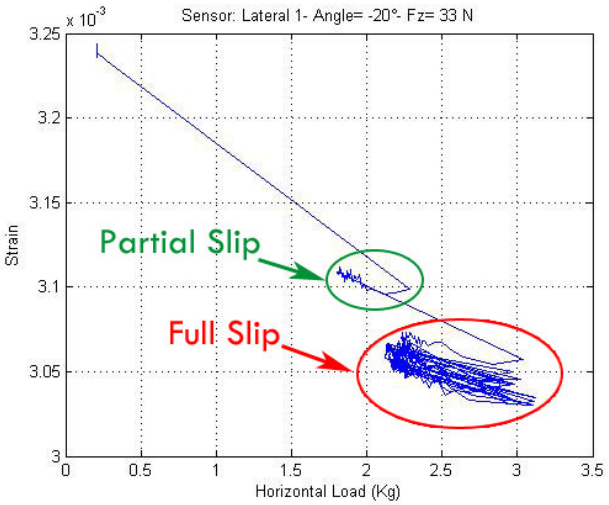


Fig. 11. Slip region detected in the horizontal load- strain relationship for a lateral sensor.

slipping. Second, when the value of Fx increases, the tread blocks become almost straight with respect to the slide and this is when the slide starts to slip on the tyre. From this moment onwards, the slide slips on the contacting blocks each time Fx is applied.

Two additional points can be mentioned about the relationships in Fig. 10 and Fig. 11. First, only the first portion of these relationships, i.e., from horizontal load= 0 kg up to where the measurements start to be stacked together, contains the important information since the rest of the figure is nothing but a repetition. Second, it is perceived that the magnitude of the horizontal load which initiates the slippage phase is higher than the magnitude which maintains the slippage afterwards.

Fig. 15 compares the sensors' readings in terms of the values of Fx which initiate the full slip at different vertical forces. This figure illustrates that the sensors deliver very similar results; therefore, it is concluded that the strain sensors can detect the start of the full slip region with a high degree of consistency. The readings of the sensor called Lateral 2 is not presented in this figure as it stopped working after a number of tests.

Another interesting observation in Fig. 15 is that as the magnitude of the applied vertical force (Fz) increases, the value of the horizontal force (Fx) which is required to make the tyre starts slipping increases too. As can be envisioned, the heavier the tyre is, the more contact it will hold with the road and thereby a higher horizontal force is needed to force it to slip.

Finally, it is worth mentioning that the horizontal load-strain measurements relationships at different angles were used to construct the strain profiles required for the algorithms presented in section 3. In details, from Fig. 10 and Fig. 11, the value of the strain at a particular horizontal load was recorded. This operation was repeated for the other angular positions. As a result, the strain profiles were concluded for different values of Fx and Fz. Fig 16 and

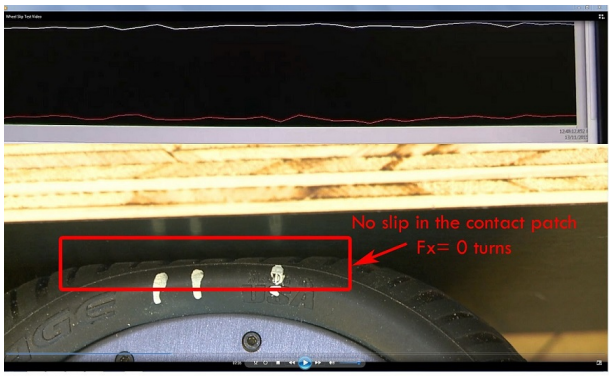


Fig. 12. Screenshot Fx= 0 turns.


Fig. 13. Screenshot Fx= 1 turns.

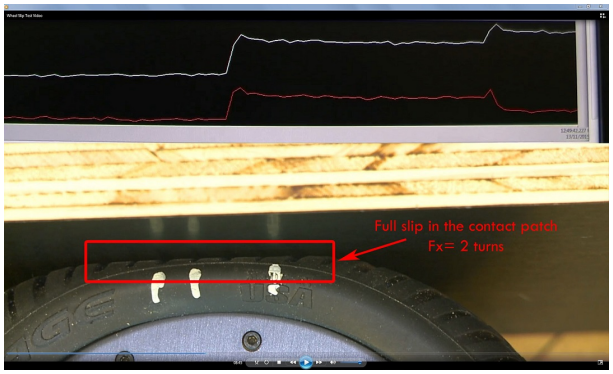


Fig. 14. Screenshot Fx= 2 turns.

Fig 17 show an example of these profiles for a longitudinal and a lateral sensor, respectively. In this Figure, assuming that angle $0°$ is the centre of the contact patch, slight changes in strain values are noticed in the angles far from the contact patch at both sides, i.e., angles $-120°$ to $-60°$ and $60°$ to $120°$. On the contrary, such variations become more significant in the vicinity of the contact patch, namely, at angles $-60°$ to $60°$. Same observations about strain changes were reported by [19]. These strain variations are attributed to corresponding deformations around tyre circumference. The part of the tyre which makes contact with the ground is the most deformed since it endures effects of applied forces. Therefore, the strain changes are higher within and near the tyre contact patch.

As described in the algorithms in section 3, finding the

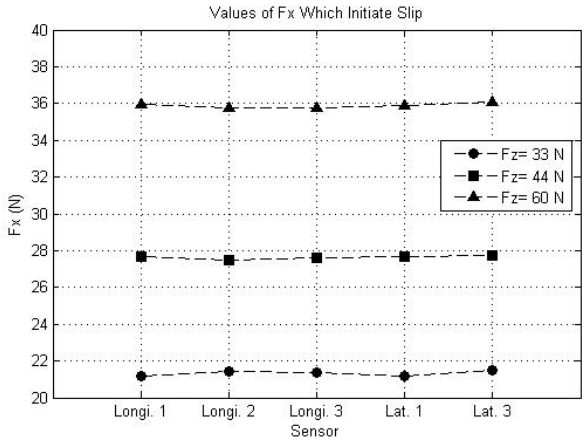


Fig. 15. Comparing the sensors' readings in terms of Fx values which initiate slip at different Fz values (Longi.= Longitudinal, Lat.= Lateral, Lateral 2 is not presented because it has malfunctioned).

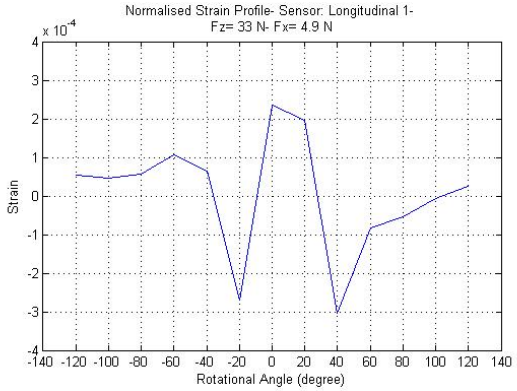


Fig. 16. Example of a strain profile collected by a longitudinal strain sensor.

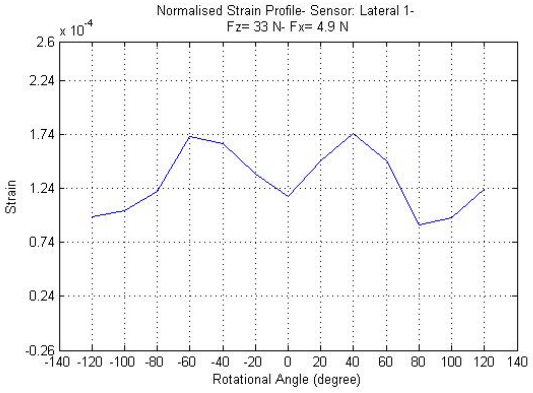


Fig. 17. Example of a strain profile collected by a lateral strain sensor.

strain profiles leads to estimating the applied longitudinal force, vertical force, longitudinal slip ratio, longitudinal slip's displacement and direction, lateral force, slip angle, and lateral slip's displacement and direction.

## VII. CONCLUSIONS AND FUTURE WORKS

### A. *Conclusions*

This paper has presented a modern sensing technique, which utilizes sensors mounted inside tyres, to directly monitor tyres' forces and slip variables for robotic platforms. The

paper also showed the potential of utilising the readings of this sensing system to construct relationships which link the sensors' measurements to longitudinal forces, vertical forces, lateral forces, slip angle, and slip ratio. The implemented sensor design was examined with static tests using a bench-top rig. These tests showed promising results because they indicated that the sensors can detect slip with a consistent performance. The sensor system was robust in its ability to identify slip incidents regardless of the angular position of the sensors as well as the applied horizontal and vertical loads.

### *B. Future Works*

Future work will focus on developing a deeper analysis for the results of these static tests to extract useful information for wheel slip estimation. Later on, advanced, dynamic tests will be undertaken to evaluate the performance of the sensor design and the slip estimation method in various working conditions.

## VIII. ACKNOWLEDGMENTS

This work has been supported by the University of Southern Queensland. The senior author would like to acknowledge the University of Technology, Baghdad, Iraq for funding the PhD scholarship.

## REFERENCES

[1] H. Chae and J. Song, "Slippage detection and pose recovery for upward-looking camera-based slam using optical flow," *in 13th Int. Conf. Control, Automation and Systems (ICCAS)*, Gwangju, Korea, October 20-23 , 2013, pp. 1108–1113.

[2] C. C. Ward and K. Iagnemma, "A dynamic-model-based wheel slip detector for mobile robots on outdoor terrain," *IEEE Trans. Robotics*, vol. 24, no. 4, pp. 821–831, 2008.

[3] X. Song, Z. Song, L. D. Seneviratne, and K. Althoefer, "Optical flow-based slip and velocity estimation technique for unmanned skid-steered vehicles," *in IEEE/RSJ Int. Conf. Intelligent Robots and Systems*, Nice, France, September 22-26, 2008, pp. 101–106.

[4] S. C. Ergen, A. Sangiovanni-Vincentelli, X. Sun, R. Tebano, S. Alalusi, G. Audisio, and M. Sabatini, "The tire as an intelligent sensor," *IEEE Trans. Computer-Aided Design of Integrated Circuits and Systems*, vol. 28, no. 7, pp. 941–955, July 2009.

[5] J. Yi, H. Wang, J. Zhang, D. Song, S. Jayasuriya, and J. Liu, "Kinematic modeling and analysis of skid-steered mobile robots with applications to low-cost inertial-measurement-unit-based motion estimation," *IEEE Trans. Robotics*, vol. 25, no. 5, pp. 1087–1097, October 2009.

[6] D. Krier, G. S. Zanardo, and L. del Re, "A pca-based modeling approach for estimation of road-tire forces by in-tire accelerometers," *in 19th World Congress, The International Federation of Automatic Control (IFAC)*, Cape Town, South Africa, August 24-29 , 2014, pp. 12029–12034.

[7] M. E. Palmer, C. C. Boyd, J. McManus, and S. Meller, "Wireless smart tires for road friction measurement and self state determination," *in 43rd AIAA/ASME/ASCE/AHS Structures, Structural Dynamics, and Materials Conference*, Denver, Colorado, April 22-25, 2002, Paper AIAA-2002-1548.

[8] A.J. Tuononen, "Optical position detection to measure tyre carcass deflections," *Vehicle System Dynamics*, vol. 46, no. 6, pp. 471–481, 2008.

[9] G. Erdogan, L. Alexander, and R. Rajamani, "Estimation of tire-road friction coefficient using a novel wireless piezoelectric tire sensor," *IEEE Sensors Journal*, vol. 11, no. 2, pp.267–279, 2011.

[10] T. Ise, M. Higuchi, and H. Tachiya, "Development of a tactile sensor to measure tire friction coefficients in arbitrary directions," *International Journal of Automation Technology*, vol. 7, no. 3, pp. 359– 366, 2013.

[11] R. Matsuzaki, N. Hiraoka, A. Todoroki, and Y. Mizutani, "Strain monitoring and applied load estimation for the development of intelligent tires using a single wireless ccd camera," *in J. Solid Mechanics and Materials Engineering*, vol. 6, no. 9, pp. 935–949, 2012.

[12] R. D. Moffitt, S. M. Bland, M. R. Sunny, and R. K. Kapania, "Sensor technologies for direct health monitoring of tires," *Encyclopedia of Structural Health Monitoring*, John Wiley Sons, Ltd., ISBN: 978-0-470-05822-0, 2008.

[13] Y. Xiong and A. Tuononen, "A laser-based sensor system for tire tread deformation measurement," *Measurement Science and Technology*, vol. 25, no. 11, Paper 115103, 2014.

[14] J. Yi, "A piezo-sensor-based smart tire system for mobile robots and vehicles," *IEEE/ASME Trans. Mechatronics*, vol. 13, no. 1, pp. 95–103, February 2008.

[15] Y. Zhang,J. Yi, and T. Liu, "Embedded flexible force sensor for in-situ tire-road interaction measurements," *IEEE Sensors J.*, vol. 13, no. 5, pp. 1756–1765, May 2013.

[16] S. M. Savaresi, M. Tanelli, P. Langthaler, and L. Del Re, "New Regressors for the Direct Identification of Tire Deformation in Road Vehicles Via In-Tire Accelerometers," *IEEE Trans. Control Systems Technology*, vol. 16, no. 4, pp. 769–780, July 2008.

[17] R. Matsuzaki and A. Todoroki, "Intelligent tires based on measurement of tire deformation," *in Journal of solid mechanics and Materials engineering*, vol. 2, no. 2, pp. 269–280, 2008.

[18] L. Li, F. Wang, and Q. Zhou, "Integrated Longitudinal and Lateral Tire/Road Friction Modeling and Monitoring for Vehicle Motion Control," *IEEE Trans. Intelligent Transportation Systems*, vol. 7, no. 1, pp. 1–19, March 2006.

[19] X. Yang, "Finite element analysis and experimental investigation of tyre characteristics for developing strain-based intelligent tyre system," Ph.D. dissertation, Dept. Mech. Eng., The University of Birmingham, Birmingham, UK, September 2011.